IJC Heart & Vasculature 9 (2015) 1–10

Contents lists available at ScienceDirect

IJC Heart & Vasculature

journal homepage: http://www.journals.elsevier.com/ijc-heart-and-vasculature

Left ventricular deformation and torsion assessed by speckle-tracking echocardiography in patients with mutated transthyretin-associated cardiac amyloidosis and the effect of diflunisal on myocardial function☆

Jun Koyama [a,*], Masatoshi Minamisawa [a], Yoshiki Sekijima [b], Shu-ichi Ikeda [b], Ayako Kozuka [a], Soichirou Ebisawa [a], Takashi Miura [a], Hirohiko Motoki [a], Ayako Okada [a], Atsushi Izawa [a], Uichi Ikeda [a]

[a] Department of Cardiovascular Medicine, Shinshu University School of Medicine, Matsumoto, Japan
[b] Department of Medicine (Neurology and Rheumatology), Shinshu University School of Medicine, Matsumoto, Japan

ARTICLE INFO

Article history:
Received 18 May 2015
Received in revised form 29 July 2015
Accepted 30 July 2015
Available online 4 August 2015

Keywords:
Mutated transthyretin
Cardiac amyloidosis
Speckle tracking echocardiography
Strain

ABSTRACT

Background: Mutated transthyretin-associated (ATTRm) amyloidosis with heart failure is associated with decreased longitudinal left ventricular (LV) myocardial contraction, as measured by strain Doppler echocardiography. We sought to clarify whether speckle-tracking echocardiography (STE) would provide useful information in patients with ATTRm cardiac amyloidosis.

Methods: One hundred twenty-three consecutive patients with ATTRm amyloidosis were divided into 3 groups. Group 1 had no evidence of cardiac involvement (n = 47), group 2 had heart involvement but no congestive heart failure (CHF) and/or serum brain natriuretic peptide (BNP) levels <100 pg/mL (n = 35), and group 3 had heart involvement and CHF and/or serum BNP levels ≥100 pg/mL (n = 41). All patients underwent standard 2-dimensional (2D), Doppler echo, and STE.

Results: By standard 2D and Doppler echo, differences in parameters were only apparent between group 3 and groups 1 and 2. Global circumferential strains by STE at each LV level and LV torsion were different between group 1 and groups 2 and 3, but not between group 2 and group 3. In contrast, global longitudinal LV strain showed significant intergroup differences (−17.3 ± 2.3%, −13.3 ± 2.3%, −9.9 ± 3.3% for groups 1 to 3, respectively, $P < 0.0001$). Radial strain also showed significant intergroup differences for each basal LV segment. Among 41 patients who could have been followed up after 1 year, 34 patients with diflunisal treatment had shown improvement in apical rotation and torsion without deterioration in multidirectional strains.

Conclusion: ATTRm cardiac amyloidosis is characterized by progressive impairment in longitudinal and basal LV radial function when global circumferential shortening and torsion remain unchanged.

1. Introduction

Cardiac amyloidosis is a cardiomyopathy associated with thickening of all 4 chambers, with biatrial dilation, a normal or mildly dilated right ventricle, and normal or decreased left ventricular (LV) cavity size. Congestive heart failure (CHF) may occur even if LV ejection fraction is normal [1–7]. Therefore, it is generally considered that CHF in cardiac amyloidosis manifests predominantly as diastolic LV dysfunction, with systolic dysfunction only occurring late in the disease [5,8–12]. Tissue Doppler echocardiography has demonstrated that cardiac amyloidosis is characterized by early impairment of systolic function at a time when fractional shortening remains normal, and that this abnormality precedes the onset of CHF [13,14]. Speckle tracking echocardiography (STE) allows the evaluation of different components of complex cardiac motions, such as longitudinal, circumferential, and radial strain, and rotation [15–18].

Many studies have focused on light-chain associated cardiac amyloidosis, but few data concerning mutated transthyretin-associated (ATTRm) amyloidosis have been derived using strain echocardiography [19–21]. The purpose of this study was to clarify whether STE could detect early regional myocardial dysfunction in ATTRm amyloidosis, before the onset of CHF, and to determine whether change in regional myocardial deformation can be detected by STE in these patients after oral small-molecule treatment by diflunisal [20].

2. Methods

2.1. Study population

One hundred twenty-eight consecutive patients with ATTRm amyloidosis were examined at the Shinshu University Hospital between

☆ There is no relationship with industry to disclose.

* Corresponding author at: Department of Cardiovascular Medicine, Shinshu University School of Medicine, 3-1-1 Asahi, Matsumoto, Nagano 390-8621, Japan.
E-mail address: jkoyama@shinshu-u.ac.jp (J. Koyama).

http://dx.doi.org/10.1016/j.ijcha.2015.07.010

January 2003 and March 2011. The diagnosis of amyloidosis was made by biopsy of involved organs, which demonstrated the typical Congo-red birefringence when viewed under polarized light. ATTRm amyloidosis was diagnosed from amyloid deposition in the abdominal fat pad (n = 90), endocardium (n = 10), stomach (n = 6), duodenum (n = 5), and rectum (n = 7), skin (n = 4), sural nerve (n = 4), vitreum (n = 3), and from the biopsy of carpal tunnel (n = 1) (there are overlap in some patients). Additionally, TTR gene analysis was routinely carried out, as previously described [22,23].Patients with atrial fibrillation (n = 5) were not included. Thus the final population consisted of 123 patients.

All patients underwent a physical examination by cardiologists, with particular emphasis on the signs and symptoms of CHF, or a chest radiographic appearance of heart failure and/or the presence of elevated jugular venous pressure with peripheral edema [13,14,24–26]. Echocardiograms were reviewed by 2 readers to determine the degree of cardiac involvement, defined as a mean LV wall thickness >12 mm in the absence of hypertension, valvular heart disease, or criteria for LV hypertrophy on the electrocardiogram [6,7,13,14, 24–26]. Some patients, who were not indicated for liver transplantation (n = 41), had been prescribed diflunisal, which prevents amyloidogenesis in vitro [27], and these patients were examined before and 1 year after starting the medication. Of these 41 patients, 7 patients discontinued diflunisal administration because of transient acute deterioration of renal function. Plasma levels of brain natriuretic peptide (BNP) were measured on the day of echocardiography, as previously described [28].

Seventy-six patients met the echocardiographic criteria for cardiac involvement, and 47 had no features of cardiac amyloidosis. The latter group was defined as group 1 (noncardiac amyloid), as we described previously [13,14,24–26]. Some patients with ATTRm had gait impairment due to peripheral nerve neuropathy, which limits behavior and masks CHF symptoms. In such patients, plasma BNP levels ≥100 pg/mL were taken as the criterion for CHF. Of the 76 patients with cardiac amyloidosis, 41 had prior or current evidence of CHF or plasma BNP levels ≥100 pg/mL [29]. These patients were defined as group 3 (CHF [+]), and the remaining 35 were defined as group 2 (CHF [−]).

Positive findings of 99mTc-PYP accumulation in the heart were also used to define groups 2 and 3 (cardiac amyloid).

2.2. Standard echocardiography

Ultrasound examinations were performed using a Vivid 7 System echocardiograph (General Electric Healthcare, Milwaukee, WI, USA) with a 1.5–4.0 MHz (M3S) transducer. Standard M-mode measurements of the LV were made. The LV end-diastolic and end-systolic volumes, ejection fraction, and left atrial (LA) maximum and minimum volumes were measured as previously described [30]. Transmitral, pulmonary venous, and LV outflow tract flow velocities were measured by pulsed Doppler echocardiography as previously described [13,14,24, 26–30]. Pulsed tissue Doppler imaging was performed using harmonic imaging, and the gate length of regions of interest was set at 0.59 cm. Sample volumes were placed on the basal interventricular septum and basal lateral walls, as described previously [13].

2.3. Speckle tracking echocardiography

Two-dimensional black-and-white cardiac cycle acquisitions were recorded in apical 2-chamber and 4-chamber views, apical long-axis view, and parasternal short-axis view (at base, mid, and apex), and stored on a hard drive. Three consecutive beats were stored in each view during breath-hold at a frame rate of 70–97 frames/s. Speckle-tracking analysis was performed offline by commercially available software (Echo Pac PC ver. 112; GE Vingmed Ultrasound, AS, Horten, Norway). After manual tracing of the endocardial border at end systole for apical and short-axis views, a region of interest was manually adjusted to include the entire myocardial thickness. The LV global and segmental longitudinal 2-dimensional strains were assessed in the apical 2-chamber, 4-chamber, and long-axis views by automated function imaging. Global and segmental longitudinal strain rates were measured from 3 apical views, and the values were averaged. LV global circumferential strain (GCS) and strain rate were measured in the parasternal short-axis view at basal, mid, and apical LV.

Segmental circumferential strain, strain rate, LV radial strain (RS), and strain rate were calculated for 6 segments (anteroseptal, anterior, lateral, posterior, inferior, and septal walls) in the parasternal short-axis view at basal, mid, and apical LV.

Measurement of LV rotation and torsion was performed as previously described [18].

Peak systolic LV torsion was calculated as the maximum instantaneous difference between peak systolic apical and basal rotation, using the R-peak in the electrocardiogram as a reference point. For LV torsion rate, the peak systolic, peak early diastolic, and peak late diastolic values were measured. In the follow-up echocardiographic assessment 1 year after the initial examination, each echocardiographic movie was recorded at the same frame rate, depth, and cut plane as with the previous picture.

2.4. Intraobserver and interobserver reproducibilities

To test the intraobserver reproducibility of the strain, strain rate, rotation, and torsion variables, 20 randomly selected patients were reviewed by the same observer >2 weeks after the first measurements. To test interobserver reproducibility, measurements were repeated by a second observer. The bias (mean difference) and limits of agreement between the first and second measurements were determined. To assess [18] reproducibility, the coefficient of variation was calculated as the standard deviation of the difference divided by the mean.

2.5. Statistical analyses

The normal distribution of continuous variables was checked using the Shapiro–Wilk W test, and all data were then expressed as mean ± standard deviation (SD). Categorical variables were expressed as absolute numbers and percentages. Statistical analyses were performed using commercially available software (JMP 9.0.2, SAS Institute, Cary, North Carolina, and Graph Pad Prism 5 for Mac OS X, GraphPad, San Diego, California, USA). Differences among the 3 groups were assessed using one-way analysis of variance, with Tukey–Kramer's HSD test for parametric variables, the Kruskal–Wallis test with Dunn's post-hoc test for nonparametric variables, and the chi-square test for categorical variables. The Bland–Altman analysis was conducted to assess intra- and interobserver agreements (expressed as absolute value of mean difference ± 1.96 SD), and intraclass correlation coefficients were calculated. Follow-up data were tested by paired t test in each group. A difference or correlation was considered significant when the probability value was <0.05.

This study was approved by the Ethics Committee of the Shinshu University School of Medicine and written informed consent was obtained from each patient.

3. Results

3.1. Patients' characteristics

The clinical characteristics are shown in Table 1. The age was greater in groups 2 and 3 compared to group 1. There were more men in group 2 than the other 2 groups. Most patients (92.7%) which entered this study had the same transthyretin mutation, involving the substitution of methionine for valine at position 30 (V30M). Other types of mutation were summarized in Table 1. Diastolic blood pressure was lower in group 3 than that in the other 2 groups. Heart rate in groups 2 and 3

Table 1
Clinical and echocardiographic characteristics of the patients in this study (n = 123).

Variable	Group 1 Mean LV thickness < 12 mm (n = 47)	Group 2 CHF(−) and BNP < 100 pg/mL (n = 35)	Group 3 CHF(+) or BNP ≥ 100 pg/mL (n = 41)
Age, year	44 ± 13	62 ± 12*	63 ± 12*
Gender (male/female), n	22/25	26/9	19/22
Type of mutation V30M/non-V30M	47/0	34/1 (S50R)	33/8 [D38A (3), S50I (1), E54K (1), E42G(1), S50R (1), H88R (1)]
Systolic blood pressure, mm Hg	112 ± 10	120 ± 19	107 ± 17§
Diastolic blood pressure, mm Hg	71 ± 10	78 ± 13#	65 ± 12#,†
Heart rate, bpm	70 ± 13	61 ± 11‖	61 ± 11‡
Left atrial diameter, cm	3.33 ± 0.47	4.09 ± 0.67*	4.24 ± 0.70*
Left atrial volume max, mL	48 ± 18	68 ± 28‖	81 ± 28*,**
Left atrial volume min, mL	21 ± 10	34 ± 20#	54 ± 27*,†
Left atrial emptying fraction, %	56 ± 9	52 ± 9	36 ± 14*,†
LV end-diastolic diameter, cm	4.35 ± 0.42	4.37 ± 0.46	4.30 ± 0.48
LV end-systolic diameter, cm	2.52 ± 0.38	2.69 ± 0.35	2.80 ± 0.49‖
LV fractional shortening, %	42.2 ± 6.9	38.5 ± 5.5	34.9 ± 7.1*,§
LV thickness (septum), cm	1.00 ± 0.15	1.63 ± 0.30*	1.92 ± 0.39*,†
LV thickness (posterior), cm	0.92 ± 0.16	1.38 ± 0.24*	1.66 ± 0.32*,†
LV end-diastolic volume, mL	50 ± 15	54 ± 11	56 ± 16
LV end-systolic volume, mL	19 ± 6	21 ± 5	25 ± 9‡
LV ejection fraction, %	62 ± 5	61 ± 5	55 ± 10‡,§
Plasma BNP, pg/mL	30.3 ± 25.0	48.0 ± 24.6	315.5 ± 282.4*,†

* $P < 0.0001$ vs. group 1.
† $P < 0.0001$ vs. group 2.
‡ $P < 0.001$ vs. group 1.
§ $P < 0.01$ vs. group 2.
‖ $P < 0.01$ vs. group 1.
\# $P < 0.05$ vs. group 1.
** $P < 0.05$ vs. group 2.

was lower than that in group 1. Plasma BNP levels were greater in group 3 than that in the other 2 groups.

3.2. Two-dimensional echocardiography

LA diameter was greater in groups 2 and 3 than that in group 1. Maximum and minimum LA volumes were larger in group 2 than group 1, and larger in group 3 than that in group 2. LA emptying fraction in group 3 was significantly lower than that in the other 2 groups. The LV end-diastolic diameter and volume showed no significant difference among the 3 groups, but the LV end-systolic diameter and volume were greater in group 3 than those in the other 2 groups, and the LV fractional shortening and ejection fraction were smaller in group 3 than those in the other 2 groups.

3.3. Standard Doppler flow and pulsed tissue Doppler

Transmitral flow, pulmonary venous flow, and LV outflow tract flow data are shown in Table 2. Patients in group 3 showed abnormal values in transmitral flow, pulmonary venous flow parameters, and isovolumic contraction time compared to those in groups 1 and 2. Patients in group 2 showed smaller values of peak E velocity of transmitral flow, but greater values of peak A wave, deceleration time of transmitral flow, isovolumic relaxation time, and ejection time compared to those in the other 2 groups. Patients in group 3 showed smaller values of transmitral peak A-wave velocity, peak S, and peak A velocity of pulmonary venous flow compared to those in groups 1 and 2.

Pulsed tissue Doppler velocity of the mitral annulus (s′, e′, and a′) and E/e′ at the septal and lateral walls was smaller in group 2 than that in group 1, and smaller in group 3 than that in group 2. E/e′ ratio at the septal and lateral walls was greater in group 2 than that in group 1, and greater in group 3 than that in group 2.

3.4. LV rotational measurements

Rotation and rotation rate (S, E, A) in basal LV did not show significant intergroup differences (Table 3). The rotation in mid-LV showed smaller values in groups 2 and 3 than that in group 1. There were no significant differences in rotation rate (S, E, A) in mid-LV among the 3 groups. The rotation and rotation rate (S) in apical LV were lower in group 3 than those in group 1, and rotation rate (E) in groups 2 and 3 was less than that in group 1. LV torsion was smaller in group 3 than that in group 1, and torsion rate (S, A) was smaller in group 3 than that in the other 2 groups. The rotation rate (E) was smaller in group 2 than that in group 1.

3.5. Global left ventricular strain and strain rate

GLS and systolic strain rate (S) were superior in detecting differences among the 3 groups (Table 4). The values of early diastolic longitudinal strain rate (E) in group 2 were smaller than those in group 1, whereas those in group 3 were similar to those in group 2. The values of late diastolic longitudinal strain rate (A) in group 2 were similar to those in group 1, and were lower in group 3 than those in the other 2 groups. The values of global circumferential strain, systolic strain rate (S), and early diastolic strain rate (E) in group 2 were smaller than those in group 1, whereas those in group 3 were preserved as those in group 2. These tendencies were observed at all (basal, mid-, and apical) LV levels. On the other hand, the values of global late diastolic strain rate (A) in group 2 were similar to those in group 1, whereas those in group 3 were lower than those in the other 2 groups. The values of mean radial strain, and early diastolic strain rate (E) were superior in detecting differences among the 3 groups at basal LV, whereas there was no difference in radial strain in apical LV. The value of mean radial strain rate (S), (A) separates group 3 from groups 1 and 2 in basal, mid-, and apical LV.

3.6. Segmental left ventricular strain and strain rate

Fig. 1A–C show segmental LV longitudinal strain and strain rate calculated from the septal, lateral, inferior, anterior, posterior, and anteroseptal walls in the basal, mid, and apical left ventricle. Strain and strain rate documented that an increased wall thickness was associated with a decrease in systolic parameters in group 2 (no CHF) at the base and mid-LV. In addition, group 3 had greater abnormalities of

Table 2
Doppler flow and pulsed tissue Doppler data (mean ± SD).

Variable	Group 1 (n = 47)	Group 2 (n = 35)	Group 3 (n = 41)
Transmitral flow peak E velocity, m/s	0.84 ± 0.22	0.69 ± 0.24[#]	0.85 ± 0.21[§]
Transmitral flow peak A velocity, m/s	0.71 ± 0.17	0.83 ± 0.19[#]	0.61 ± 0.25[#,†]
Transmitral flow peak E/A	1.23 ± 0.43	0.89 ± 0.54	1.84 ± 1.34[‖,†]
Deceleration time of transmitral flow, ms	203 ± 49	281 ± 75[*]	232 ± 68[§]
Transmitral flow A duration, ms	149 ± 22	169 ± 24[‖]	164 ± 30[‖]
Pulmonary venous flow peak S velocity, m/s	0.53 ± 0.13	0.56 ± 0.15	0.43 ± 0.20[‖,§]
Pulmonary venous flow peak D velocity, m/s	0.45 ± 0.09	0.38 ± 0.14	0.57 ± 0.19[‡,†]
Pulmonary venous flow peak A velocity, m/s	0.30 ± 0.06	0.34 ± 0.13	0.26 ± 0.13[§]
Pulmonary venous flow peak D/S	0.90 ± 0.25	0.80 ± 0.73	1.86 ± 1.59[*,†]
Pulmonary venous flow D velocity deceleration time, ms	283 ± 287	339 ± 123	254 ± 79
Pulmonary venous flow A duration, ms	157 ± 24	184 ± 41[‖]	184 ± 34[*]
Left ventricular outflow tract peak velocity, m/s	0.98 ± 0.16	0.95 ± 0.17	1.00 ± 0.20
Left ventricular outflow tract mean velocity, m/s	0.64 ± 0.10	0.64 ± 0.12	0.66 ± 0.14
Left ventricular outflow tract velocity time integral, cm	19.3 ± 3.9	20.3 ± 3.4	19.5 ± 4.3
Isovolumic contraction time, ms	82 ± 17	94 ± 21	109 ± 29[*,§]
Isovolumic relaxation time, ms	87 ± 20	122 ± 31[‡]	109 ± 46[‖]
Ejection time, ms	294 ± 38	317 ± 39[#]	294 ± 31[§]
Tissue Doppler imaging (peak systolic: s′, septum), cm/s	6.45 ± 1.33	5.05 ± 1.05[*]	3.63 ± 1.31[*,†]
Tissue Doppler imaging (peak early diastolic: e′, septum), cm/s	6.43 ± 2.04	3.10 ± 1.14[*]	2.40 ± 0.90[*,**]
Tissue Doppler Imaging (peak late diastolic: a′, septum), cm/s	6.45 ± 1.40	5.84 ± 1.26	3.25 ± 1.91[*,†]
Tissue Doppler Imaging (peak systolic: s', lateral wall), cm/s	7.78 ± 2.10	5.76 ± 1.73[*]	4.27 ± 1.52[*,§]
Tissue Doppler Imaging (peak early diastolic: e′, lateral wall), cm/s	8.77 ± 2.65	4.63 ± 1.72[*]	3.34 ± 1.35[*,**]
Tissue Doppler Imaging (peak late diastolic a′, lateral wall), cm/s	5.99 ± 1.56	5.72 ± 1.30	3.07 ± 1.66[*,†]
E/e′ (septum)	14.0 ± 5.1	24.1 ± 9.2[‖]	39.8 ± 19.6[*,†]
E/e′ (lateral wall)	10.2 ± 3.7	17.0 ± 8.4[‖]	29.4 ± 12.9[*,†]

[*] $P < 0.0001$ vs group 1.
[†] $P < 0.0001$ vs group 2.
[‡] $P < 0.001$ vs group 1.
[§] $P < 0.01$ vs group 2.
[‖] $P < 0.01$ vs group 1.
[#] $P < 0.05$ vs group 1.
[**] $P < 0.05$ vs group 2.

strain and peak systolic strain rate (S) than those in group 2 at all sites in basal and mid-LV. Contrary to the findings for basal and mid-LV, apical longitudinal strain in lateral, anterior, and posterior walls was preserved similarly to those in groups 1 and 2.

Fig. 2A–C show circumferential and radial strain/strain rate calculated from anteroseptal, anterior, lateral, posterior, inferior, and septal walls in basal, mid, and apical LV. In the basal LV, circumferential strain (other than in lateral and posterior walls) and strain rate (S, E, and A) in all 6 segments in group 3 showed lower values than in the other 2 groups. Furthermore, strain rate (S and A) in group 2 were preserved similarly to those in group 1. These tendencies were observed in the

Table 3
Left ventricular (LV) rotational data.

Variable	Group 1 (n = 47)	Group 2 (n = 35)	Group 3 (n = 41)
Basal LV rotation (°)	−2.0 ± 4.4	−3.7 ± 3.9	−2.1 ± 2.8
Basal rotation rate (S) (°/s)	−20.4 ± 61.9	−29.7 ± 44.6	−17.0 ± 28.9
Basal rotation rate (E) (°/s)	34.4 ± 47.5	37.4 ± 47.5	15.6 ± 25.0
Basal rotation rate (A) (°/s)	20.8 ± 42.7	25.8 ± 30.3	12.9 ± 20.3
Mid-LV rotation (°)	2.5 ± 4.7	−0.3 ± 4.6[‡]	0.3 ± 3.3[‡]
Mid- rotation rate (S) (°/s)	16.9 ± 52.5	−0.5 ± 51.0	−1.0 ± 34.4
Mid- rotation rate (E) (°/s)	−17.0 ± 63.2	2.9 ± 55.8	−0.8 ± 32.5
Mid- rotation rate (A) (°/s)	−10.8 ± 41.0	7.1 ± 46.9	2.9 ± 21.1
Apical LV rotation (°)	7.4 ± 4.9	5.3 ± 3.8	5.0 ± 3.5[†]
Apical rotation rate (S) (°/s)	64.3 ± 48.3	49.3 ± 35.0	39.3 ± 26.3[†]
Apical rotation rate (E) (°/s)	−67.6 ± 46.9	−45.1 ± 42.1[‡]	−36.7 ± 26.0[*]
Apical rotation rate (A) (°/s)	−26.1 ± 38.7	−24.0 ± 34.3	−14.6 ± 18.3
LV torsion (°)	10.0 ± 5.3	8.7 ± 4.5	7.0 ± 3.3[†]
LV torsion rate (S) (°/s)	79.1 ± 40.9	73.8 ± 38.8	53.7 ± 16.2[*,§]
LV torsion rate (E) (°/s)	−93.9 ± 56.4	−61.7 ± 54.7[†]	−49.5 ± 21.2[*]
LV torsion rate (A) (°/s)	−42.4 ± 34.2	−42.0 ± 41.6	−25.3 ± 17.5[†,‖]

[*] $P < 0.0001$ vs. group 1.
[†] $P < 0.01$ vs. group 1.
[‡] $P < 0.05$ vs. group 1.
[§] $P < 0.01$ vs. group 2.
[‖] $P < 0.05$ vs. group 2.

Table 4
Global left ventricular strain imaging data.

Variable	Group 1 (n = 47)	Group 2 (n = 35)	Group 3 (n = 41)
Global longitudinal strain (%)	−17.3 ± 2.3	−13.3 ± 2.3[*]	−9.9 ± 3.3[*,†]
Strain rate (S)(s^{-1})	−1.04 ± 0.21	−0.75 ± 0.14[*]	−0.58 ± 0.19[*,§]
Strain rate (E) (s^{-1})	1.23 ± 0.33	0.60 ± 0.19[*]	0.54 ± 0.15[*]
Strain rate (A) (s^{-1})	0.80 ± 0.23	0.81 ± 0.25	0.45 ± 0.29[*,†]
Basal global circ. strain (%)	−19.5 ± 4.4	−16.5 ± 4.1[‖]	−16.0 ± 4.1[*]
Strain rate (S) (s^{-1})	−1.32 ± 0.29	−1.19 ± 0.34	−1.07 ± 0.27[*]
Strain rate (E) (s^{-1})	1.68 ± 0.62	0.99 ± 0.43[*]	0.91 ± 0.34[*]
Strain rate (A) (s^{-1})	0.79 ± 0.31	0.77 ± 0.31	0.52 ± 0.43[‡,#]
Mid-global circ. strain (%)	−20.1 ± 4.0	−16.5 ± 6.4[‖]	−16.6 ± 3.7[‡]
Strain rate (S) (s^{-1})	−1.33 ± 0.35	−1.11 ± 0.30[‖]	−1.06 ± 0.24[*]
Strain rate (E) (s^{-1})	1.50 ± 0.48	1.02 ± 0.42[*]	0.96 ± 0.30[*]
Strain rate (A) (s^{-1})	0.86 ± 0.42	0.81 ± 0.37	0.53 ± 0.36[*,#]
Apical global circ. strain (%)	−21.9 ± 5.8	−18.5 ± 4.6[‖]	−18.3 ± 4.8[‖]
Strain rate (S) (s^{-1})	−1.54 ± 0.40	−1.23 ± 0.33[‡]	−1.13 ± 0.28[*]
Strain rate (E) (s^{-1})	1.77 ± 0.60	1.17 ± 0.37[*]	1.21 ± 0.46[*]
Strain rate (A) (s^{-1})	0.93 ± 0.44	1.14 ± 0.53	0.54 ± 0.38[*,†]
Basal mean radial strain (%)	60.0 ± 2.5	43.3 ± 3.0[*]	31.0 ± 2.0[*,#]
Strain rate (S) (s^{-1})	2.19 ± 0.80	2.01 ± 0.75	1.45 ± 0.49[*,§]
Strain rate (E) (s^{-1})	−2.39 ± 0.11	−1.71 ± 0.13[‡]	−1.07 ± 0.40[*,§]
Strain rate (A) (s^{-1})	−1.74 ± 1.04	−1.53 ± 0.73	−0.90 ± 0.60[*,§]
Mid-mean radial strain (%)	61.7 ± 25.4	42.7 ± 15.3[*]	36.3 ± 18.3[*]
Strain rate (S) (s^{-1})	2.19 ± 1.58	1.98 ± 0.85	1.53 ± 0.54[‖]
Strain rate (E) (s^{-1})	−2.55 ± 1.24	−1.64 ± 0.84[*]	−1.26 ± 0.58[*]
Strain rate (A) (s^{-1})	−1.58 ± 0.97	−1.65 ± 0.83	−0.96 ± 0.62[*,†]
Apical mean radial strain (%)	41.2 ± 23.0	37.5 ± 17.0	36.3 ± 19.2
Strain rate (S) (s^{-1})	1.82 ± 0.79	1.95 ± 0.71	1.48 ± 0.69[#,**]
Strain rate (E) (s^{-1})	−2.26 ± 0.98	−1.73 ± 0.66[‖]	−1.34 ± 0.68[*,††]
Strain rate (A) (s^{-1})	−1.14 ± 0.66	−1.66 ± 0.81[‖]	−0.91 ± 0.74[†]

[*] $P < 0.0001$ vs group 1.
[†] $P < 0.0001$ vs group 2.
[‡] $P < 0.001$ vs group 1.
[§] $P < 0.001$ vs group 2.
[‖] $P < 0.01$ vs group 1.
[#] $P < 0.01$ vs group 2.
[**] $P < 0.05$ vs group 1.
[††] $P < 0.05$ vs group 2.

mid- and apical LV. Contrary to the finding for circumferential strain, radial strain and strain rate (E) in all 6 basal LV segments clearly discriminated the 3 groups. In the mid-LV, radial strain rate (S, and A) clearly discriminated group 3 from those in groups 1 and 2, but radial strain and strain rate (E) were similar in groups 2 and 3. In the apical LV, radial strain rate (S, and A) in group 3 showed lower values than those in groups 1 and 2, although radial strain did not differ significantly among the 3 groups.

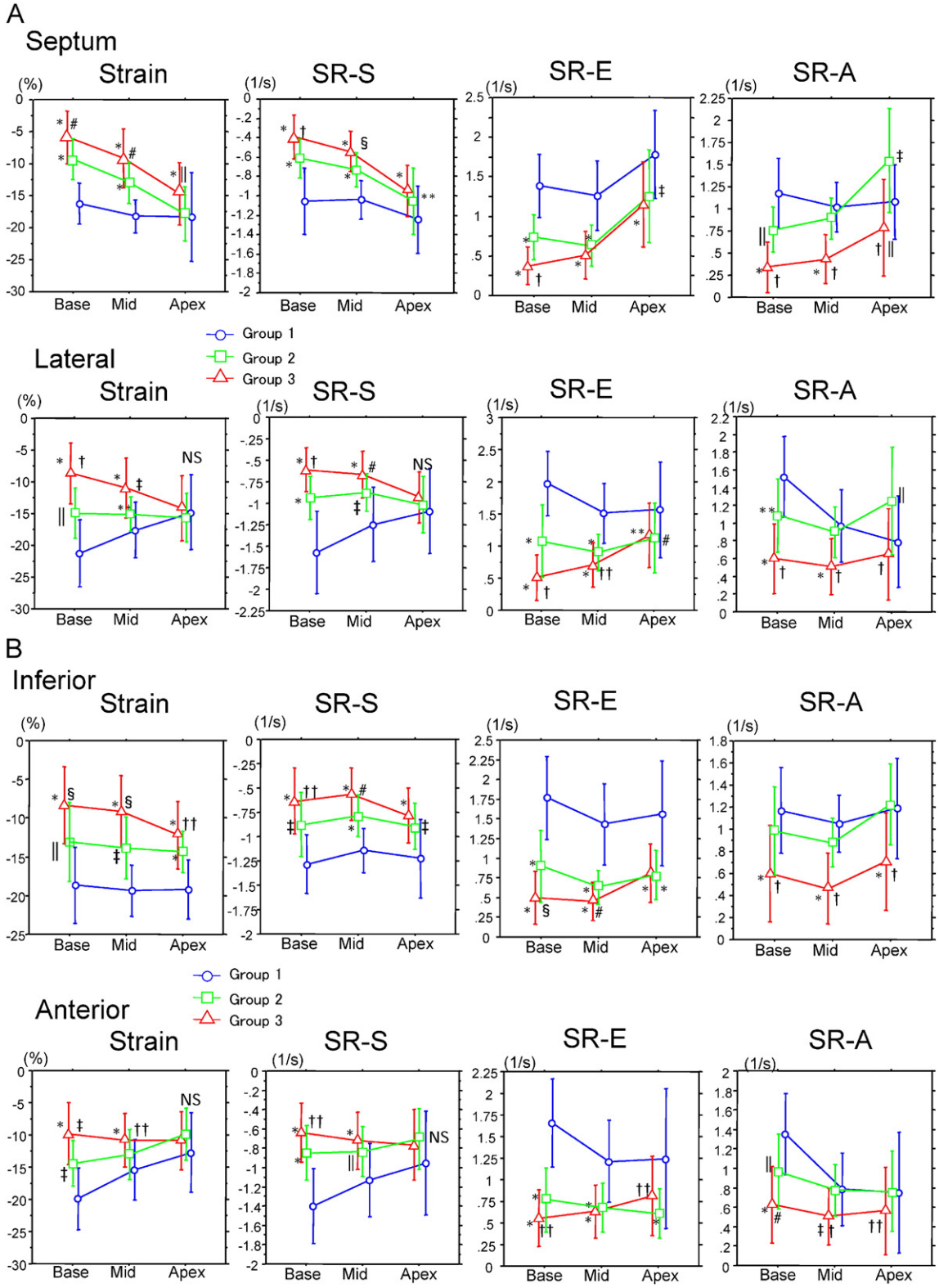

Fig. 1. Longitudinal strain, and strain rate in basal, mid-, and apical left ventricle at the septal, lateral (A), inferior, anterior (B), posterior, and anteroseptal (C) walls. Group 1, noncardiac amyloid; group 2, cardiac amyloid without CHF; group 3, CHF(+). $^{*}P < 0.0001$ vs. group 1; $^{\dagger}P < 0.0001$ vs. group 2; $^{\ddagger}P < 0.001$ vs. group 1; $^{\S}P < 0.001$ vs. group 2; $^{\|}P < 0.01$ vs. group 1; $^{\#}P < 0.01$ vs. group 2; $^{**}P < 0.05$ vs. group 1; $^{\dagger\dagger}P < 0.05$ vs. group 2; NS, not significant.

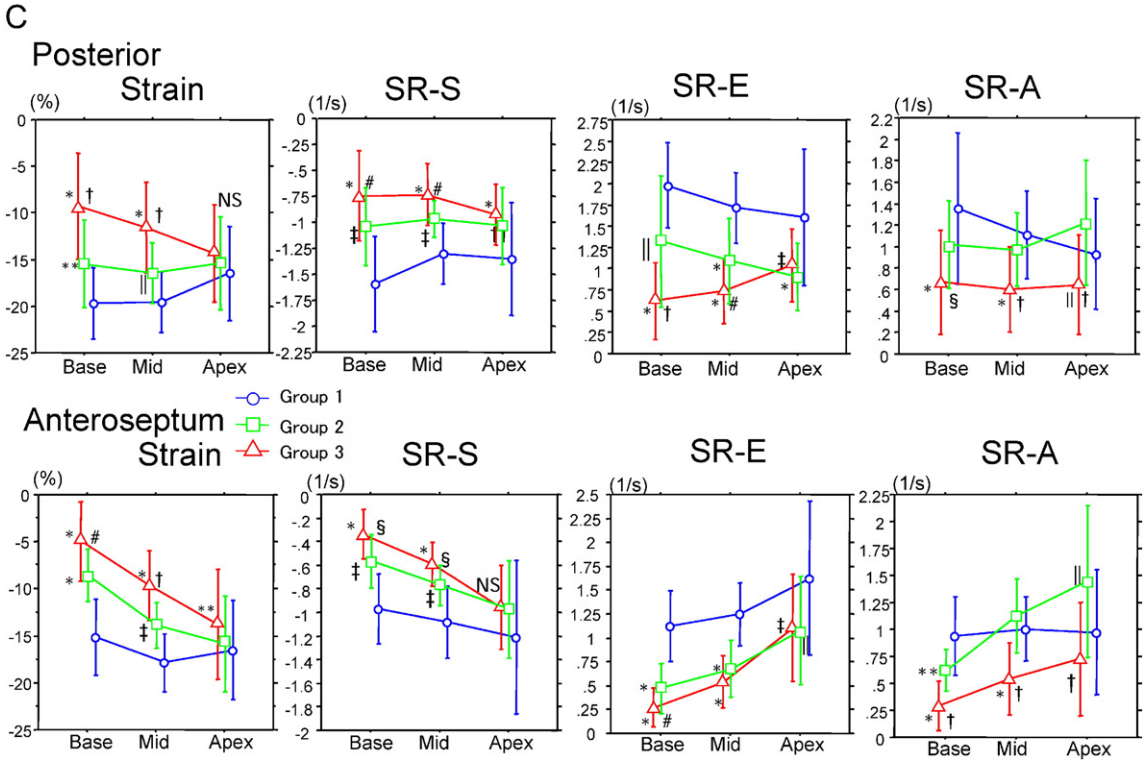

Fig. 1 (*continued*).

3.7. Follow-up data

As shown in Table 5, in the discontinued (due to transient renal dysfunction) diflunisal group (n = 7), the LV end diastolic volume was statistically decreased, the global longitudinal strain and the mean basal longitudinal strain had shown a tendency to decrease, and the mean mid-longitudinal strain, mean mid- and apical radial strains had been significantly decreased after 1 year follow-up. In contrast, the diflunisal treatment group (n = 34) showed significant improvement in the apical LV rotation and torsion without deterioration in the longitudinal, and radial strains after 1 year follow-up. Among 41 patients, no patients died during the 1 year follow-up period.

3.8. Reproducibility of measurements

Reproducibility of measurements is summarized in Table 6. Intraobserver and interobserver agreement for longitudinal, circumferential, radial strain and rotation/torsion measurements was excellent, but intraobserver and interobserver agreement for longitudinal, circumferential, and radial strain rate was poor. The coefficients of variation for intraobserver and interobserver comparisons were less than 10%.

4. Discussion

To the best of our knowledge, this study includes the maximum number of patients with ATTRm who were evaluated by speckle tracking echocardiography. We also clarify first the favorable effect of diflunisal on cardiac function in patients who were not indicated for liver transplantation. The main findings of this study were 1) ATTRm cardiac amyloidosis has a specific pattern of LV longitudinal strain, characterized by worse longitudinal strain in the basal and mid-LV with relative sparing of the apex, as we previously reported for AL cardiac amyloidosis [14,26]; 2) the radial strain shows a similar pattern to the LV longitudinal strain, i.e., a specific pattern of LV radial strain characterized by worse radial strain in the basal and mid-LV, with relative sparing of the apex; 3) circumferential strain is relatively preserved until the presence of CHF; 4) LV torsion is not increased as in true LV hypertrophy [31,32], but is relatively preserved until the onset of overt CHF signs; 5) diflunisal could be used safely even in severe cardiac amyloidosis like group 3; and 6) the follow-up study after diflunisal treatment suggested that the STE could detect subtle changes in cardiac function.

The mechanism of the specific pattern of LV longitudinal and radial strain and preserved circumferential strain may be explained by the amyloid deposition pattern in ATTRm as follows:

- Cardiac magnetic resonance with delayed gadolinium enhancement has demonstrated that the deposition of amyloid fibrils occurs from the endocardial side to the epicardial side [33].
- In the LV endocardial layer, there exist longitudinally oriented myocardial fibers, which contribute to LV longitudinal and inner LV layer radial function. Therefore, amyloid deposition in the endocardial layer might cause longitudinal systolic dysfunction, which should lead to worse longitudinal and radial LV strain.
- On the other hand, LV circumferential fiber exists in the mid-layer of LV myocardium. Therefore, circumferential LV shortening might be preserved until amyloid infiltration progresses to the mid-layer in advanced cardiac amyloidosis.

4.1. Left ventricular torsion in amyloidosis

Previous studies indicated that in patients with true LV hypertrophy, LV torsion values were significantly increased compared to normal subjects [31]. Contrary to the findings in true myocardial hypertrophy, LV torsion values were significantly decreased in advanced stages of cardiac amyloidosis. Subendocardial rotation was found to be higher than subepicardial rotation [32]. Subendocardial-dominant deposition of amyloid protein might decrease the subendocardial-dominant rotation. However, the larger moment arm of the subepicardial fibers dominates

the direction of twist, causing rotation of the apex and base in counter-clockwise and clockwise directions, respectively [34]. This may account for the relative sparing of LV torsion in the early to middle stages of cardiac amyloidosis. However, once amyloid infiltration affects the subepicardial layer in the advanced stage, LV torsion will decrease, as seen in patients with CHF.

4.2. Left atrial function in cardiac amyloidosis

We also evaluated the LA emptying fraction, which have not been described in previous reports. The LA emptying fraction decreases in CHF, whereas it is preserved in patients with LVH without CHF. This finding partially explains the higher transmitral A-wave velocity and

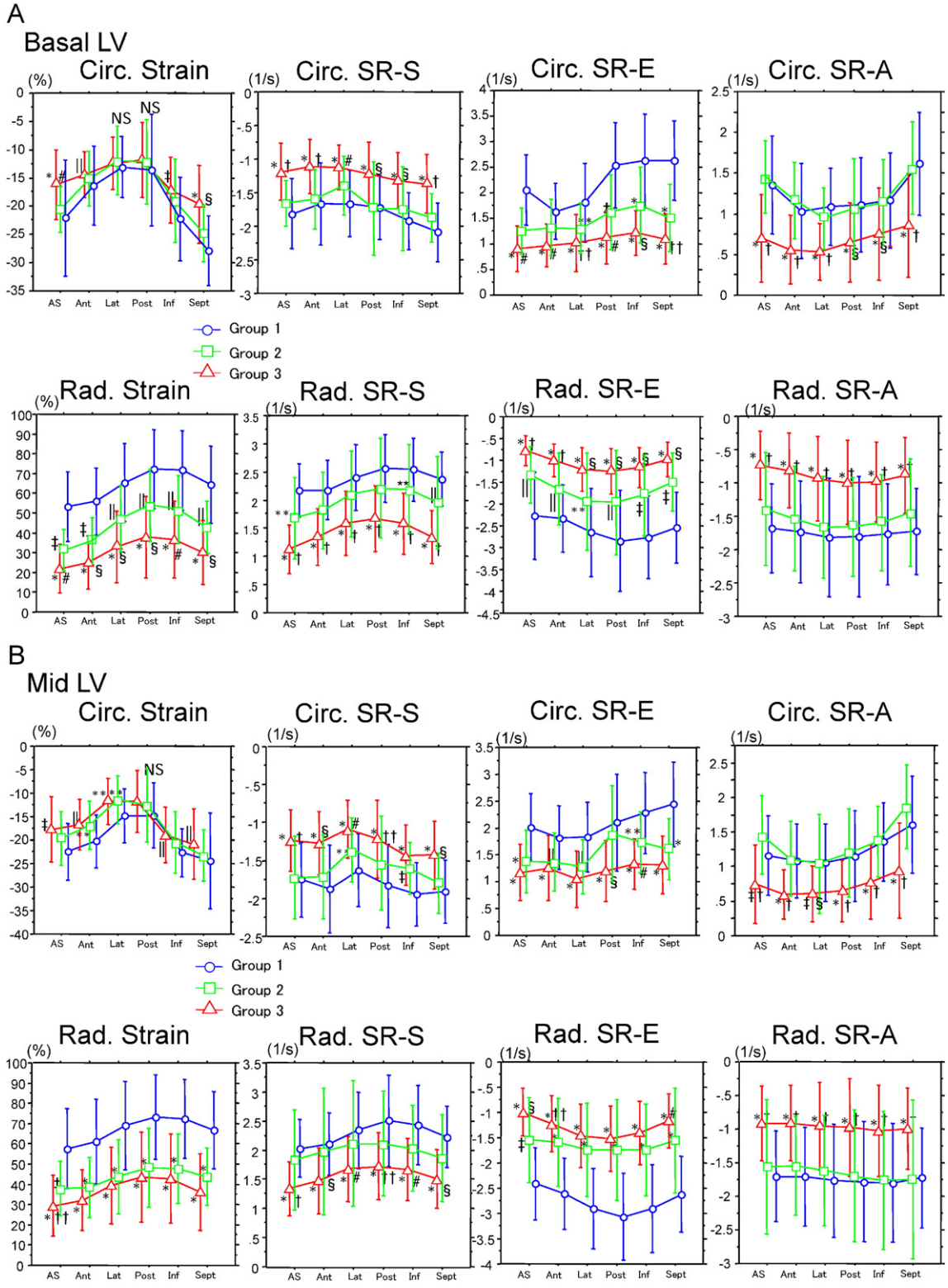

Fig. 2. Circumferential and radial strain/strain rate on basal (A), mid (B), and apical (C) left ventricle at the anteroseptal, anterior, lateral, posterior, inferior, and septal walls. Abbreviations and P-values are the same those in Fig. 1.

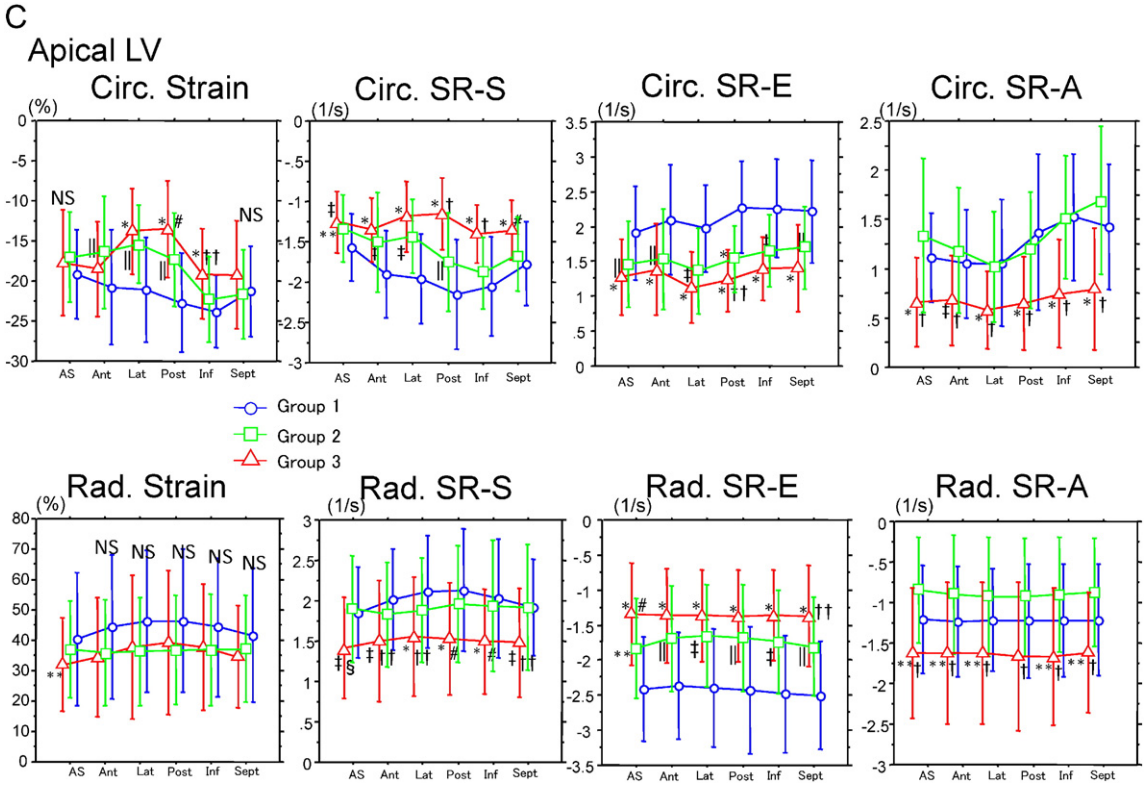

Fig. 2 (*continued*).

Table 5
Serial observation 1 year after initial echocardiographic examination.

	Pre-diflunisal (n = 34)	1 year after diflunisal	*P*	Treatment cessation due to newly developed renal dysfunction after diflunisal (n = 7)	Treatment cessation 1 year	*P*
Age, year	57 ± 16	–	–	54 ± 17	–	–
Gender (M/F), n	23/11	–	–	5/2	–	–
V30M/non-V30M	27/7	–	–	7/0	–	–
Group 1/2/3	12/7/15	–	–	3/1/3		
SBP, mm Hg	112 ± 14	111 ± 14	0.87	109 ± 11	111 ± 18	0.49
DBP, mm Hg	70 ± 12	69 ± 11	0.57	67 ± 5	72 ± 6	0.10
Heart rate, bpm	68 ± 11	64 ± 12	0.05	70 ± 8	73 ± 14	0.49
BUN, mg/dl	14.1 ± 4.9	15.8 ± 5.1	0.044	20.7 ± 9.0	24.1 ± 9.5	0.20
Creatinine, mg/dl	0.78 ± 0.21	0.83 ± 0.22	0.019	0.94 ± 0.35	0.95 ± 0.34	0.86
IVSThd, cm	1.59 ± 0.54	1.59 ± 0.53	0.94	1.75 ± 0.75	1.80 ± 0.64	0.58
LVPWThd, cm	1.33 ± 0.39	1.38 ± 0.41	0.16	1.49 ± 0.52	1.56 ± 0.51	0.12
TMF-E/A	1.15 ± 0.69	1.27 ± 0.68	0.18	1.69 ± 1.33	1.96 ± 2.1	0.54
TMF-E-DT, ms	235 ± 67	238 ± 68	0.79	188 ± 49	204 ± 50	0.62
PVF-D/S	0.98 ± 0.52	1.10 ± 0.62	0.08	1.69 ± 1.46	1.45 ± 0.97	0.54
LVOT-VTI, cm	20.2 ± 3.4	19.9 ± 3.4	0.65	15.5 ± 4.0	14.5 ± 3.4	0.44
LVEDV, mL	50 ± 16	49 ± 15	0.65	50 ± 8	40 ± 9	**0.04**
LVESV, mL	21 ± 8	20 ± 8	0.39	23 ± 8	20 ± 10	0.25
LVEF, %	60 ± 8	61 ± 7	0.43	55 ± 11	53 ± 16	0.46
BNP, pg/mL	123 ± 150	148 ± 156	0.13	200 ± 207	335 ± 365	0.26
GLS (AFI), %	−13.1 ± 3.8	−12.9 ± 4.0	0.45	−13.0 ± 6.2	−8.7 ± 5.4	**0.07**
Mean basal LS, %	−12.1 ± 5.8	−12.3 ± 5.6	0.52	−14.8 ± 7.1	−9.7 ± 5.4	**0.07**
Mean mid LS, %	−13.7 ± 4.3	−13.8 ± 4.2	0.90	−14.6 ± 6.0	−10.0 ± 5.0	**0.052**
Mean apical LS, %	−14.6 ± 3.4	−14.2 ± 3.3	0.55	−12.8 ± 4.8	−10.4 ± 4.3	0.29
Basal GCS, %	−16.6 ± 3.6	−17.1 ± 3.7	0.49	−17.1 ± 5.7	−16.4 ± 6.0	0.53
Mid GCS, %	−17.2 ± 3.6	−16.9 ± 3.9	0.68	−15.5 ± 6.2	−16.9 ± 6.7	0.22
Apical GCS, %	−17.9 ± 5.2	−18.7 ± 4.6	0.12	−18.5 ± 6.8	−16.6 ± 8.7	0.31
Mean basal RS, %	44 ± 21	40 ± 19	0.21	48 ± 25	37 ± 25	0.13
Mean mid RS, %	46 ± 21	43 ± 20	0.46	50 ± 28	34 ± 21	**0.04**
Mean apical RS, %	41 ± 20	37 ± 20	0.12	42 ± 28	32 ± 24	**0.0077**
Basal LV rotation (°)	−3.0 ± 3.7	−2.6 ± 4.2	0.68	−3.0 ± 2.4	−2.1 ± 2.8	0.52
Apical LV rotation (°)	4.8 ± 2.7	7.3 ± 3.6	**0.0012**	5.3 ± 4.4	8.7 ± 4.3	0.20
LV torsion (°)	7.5 ± 3.4	9.7 ± 5.1	**0.037**	8.4 ± 3.6	11.5 ± 4.9	0.18

No treatment, discontinued diflunisal because of deterioration in renal function after diflunisal treatment; IVSThd, LV thickness (septum); LVPWThd, LV thickness (posterior wall); TMF, transmitral flow; DT, deceleration time; PVF, pulmonary venous flow; LVOT, left ventricular outflow tract; VTI, velocity time integral; LVEDV, LV end-diastolic volume; LVESV, LV end-systolic volume; LVEF, LV ejection fraction; GLS, global longitudinal strain; AFI, automated function imaging; LS, longitudinal strain; GCS, global circumferential strain and RS, radial strain. Bold means statistically significance during 1 year follow-up.

Table 6
Reproducibility of measurements.

	Intraobserver agreement (mean ± 1.96 SD) (%)	Coefficient variation for intraobserver comparisons (%)	Interobserver agreement (mean ± 1.96 SD) (%)	Coefficient variation for interobserver comparisons (%)
Longitudinal strain	0.14 ± 1.56	5.8	0.08 ± 1.55	7.0
Circumferential strain	0.25 ± 2.0	6.1	2.6 ± 7.2	7.0
Radial strain	0.21 ± 4.9	6.2	2.2 ± 9.9	7.1
Rotation	0.02 ± 3.1	3.6	3.1 ± 3.4	9.6
Torsion	0.14 ± 2.2	9.0	2.7 ± 6.1	7.0
Longitudinal SR	0.9 ± 8.7	7.8	0.37 ± 13.8	9.8
Circumferential SR	0.3 ± 12.9	9.8	1.3 ± 16.4	9.2
Radial SR	0.22 ± 11.3	8.7	1.9 ± 22.3	8.5

SR, strain rate.

the compensatory mechanism of LA function in group 2 compared to group 1.

4.3. Limitations

Cardiac involvement was defined as a mean value of LV thickness >12 mm in patients with ATTRm amyloidosis confirmed by a biopsy from any site. Thus, many patients were diagnosed as having cardiac amyloidosis without endomyocardial biopsy. However, on the basis of autopsy studies, it generally is accepted that the echocardiographic finding of LV thickening in the absence of diseases associated with LV hypertrophy is highly specific for the finding of cardiac amyloidosis at biopsy or autopsy [35]. Furthermore, to ensure definite cardiac involvement by amyloid fibrils, we used the combined criteria with mean LV wall thickness and 99mTc-PYP scintigraphy. This method is reported to be sensitive in detecting cardiac amyloid involvement, and may assist in discriminating group 1 from groups 2 and 3.

The follow-up period was too short to evaluate the [36] effect of diflunisal treatment on cardiac function, and improvement in apical rotation and torsion without deterioration in multidirectional strains is a weak end point. Further longer follow-up study is required to confirm the results.

5. Conclusions

Transthyretin-associated cardiac amyloidosis is characterized by a progressive impairment of longitudinal and radial LV function at a time when circumferential shortening and LV torsion remain unchanged.

Disclosures

We have no conflict of interests to disclose.

References

[1] R.H. Swanton, I.A. Brooksby, M.J. Davies, D.J. Coltart, B.S. Jenkins, M.M. Webb-Peploe, Systolic and diastolic ventricular function in cardiac amyloidosis. Studies in six cases diagnosed with endomyocardial biopsy, Am. J. Cardiol. 39 (1977) 658–664.
[2] A.G. Siqueira-Filho, C.L. Cunha, A.J. Tajik, J.B. Seward, T.T. Schattenberg, E.R. Giuliani, M-mode and two-dimensional echocardiographic features in cardiac amyloidosis, Circulation 63 (1981) 188–196.
[3] M.G. St John Sutton, N. Reichek, J.A. Kastor, E.R. Giuliani, Computerized M-mode echocardiographic analysis of left ventricular dysfunction in cardiac amyloid, Circulation 66 (1982) 790–799.
[4] W.C. Roberts, B.F. Waller, Cardiac amyloidosis causing cardiac dysfunction: analysis of 54 necropsy patients, Am. J. Cardiol. 52 (1983) 137–146.
[5] L. Cueto-Garcia, G.S. Reeder, R.A. Kyle, et al., Echocardiographic findings in systemic amyloidosis: spectrum of cardiac involvement and relation to survival, J. Am. Coll. Cardiol. 6 (1985) 737–743.
[6] R.H. Falk, J.F. Plehn, T. Deering, et al., Sensitivity and specificity of the echocardiographic features of cardiac amyloidosis, Am. J. Cardiol. 59 (1987) 418–422.
[7] R.H. Falk, R.L. Comenzo, M. Skinner, The systemic amyloidoses, N. Engl. J. Med. 337 (1997) 898–909.
[8] J.R. Benotti, W. Grossman, P.F. Cohn, Clinical profile of restrictive cardiomyopathy, Circulation 61 (1980) 1206–1212.
[9] T.I. Tyberg, A.V.N. Goodyer, V.W. Hurst III, J. Alexander, R.A. Langou, Left ventricular filling in differentiating restrictive amyloid cardiomyopathy and constrictive pericarditis, Am. J. Cardiol. 47 (1981) 791–796.
[10] A.L. Klein, L.K. Hatle, D.J. Burstow, et al., Doppler characterization of left ventricular diastolic function in cardiac amyloidosis, J. Am. Coll. Cardiol. 13 (1989) 1017–1026.
[11] A.L. Klein, L.K. Hatle, C.P. Taliercio, et al., Serial Doppler echocardiographic follow-up of left ventricular diastolic function in cardiac amyloidosis, J. Am. Coll. Cardiol. 16 (1990) 1135–1141.
[12] A.L. Klein, L.K. Hatle, C.P. Taliercio, et al., Prognostic significance of Doppler measures of diastolic function in cardiac amyloidosis. a Doppler echocardiography study, Circulation 83 (1991) 808–816.
[13] J. Koyama, P.A. Ray-Sequin, R. Davidoff, R.H. Falk, Usefulness of pulsed tissue Doppler imaging for evaluating systolic and diastolic left ventricular function in patients with AL (primary) amyloidosis, Am. J. Cardiol. 89 (2002) 1067–1071.
[14] J. Koyama, P.A. Ray-Sequin, R.H. Falk, Longitudinal myocardial function assessed by tissue velocity, strain, and strain rate tissue Doppler echocardiography in patients with AL (primary) cardiac amyloidosis, Circulation 107 (2003) 2446–2452.
[15] B.H. Amundsen, T. Helle-Valle, T. Edvardsen, et al., Noninvasive myocardial strain measurement by speckle tracking echocardiography: validation against sonomicrometrys and tagged magnetic resonance imaging, J. Am. Coll. Cardiol. 47 (2006) 789–793.
[16] M.S. Suffoletto, K. Dohi, M. Cannesson, S. Saba, J. Gorcsan III, Novel speckle-tracking radial strain from routine black-and-white echocardiographic images to quantify dyssynchrony and predict response to cardiac resynchronization therapy, Circulation 113 (2006) 960–968.
[17] T. Helle-Valle, J. Crosby, T. Edvardsen, et al., New noninvasive method for assessment of left ventricular rotation: speckle tracking echocardiography, Circulation 112 (2005) 3149–3156.
[18] Y. Notomi, P. Lysyansky, R.M. Setser, et al., Measurement of ventricular torsion by two-dimensional ultrasound speckle tracking imaging, J. Am. Coll. Cardiol. 45 (2005) 2034–2041.
[19] F. Ogiwara, J. Koyama, S. Ikeda, O. Kinoshita, R.H. Falk, Comparison of the strain Doppler echocardiographic features of familial amyloid polyneuropathy (FAP) and light-chain amyloidosis, Am. J. Cardiol. 95 (2005) 538–540.
[20] F.L. Ruberg, J.L. Berk, Transthyretin (TTR) cardiac amyloidosis, Circulation 126 (2012) 1286–1300.
[21] C.C. Quarta, S.D. Solomon, I. Uraizee, et al., Left ventricular structure and function in transthyretin-related versus light-chain cardiac amyloidosis, Circulation 129 (2014) 1840–1849.
[22] S. Ikeda, T. Nakano, N. Yanagisawa, M. Nakazato, H. Tsukagoshi, Asymptomatic homozygous gene carrier in a family with type I familial amyloid polyneuropathy, Eur. Neurol. 32 (1992) 308–313.
[23] N. Tachibana, T. Tokuda, K. Yoshida, et al., Usefulness of MALDI/TOF mass spectrometry of immunoprecipitated serum variant transthyretin in the diagnosis of familial amyloid polyneuropathy, Amyloid 6 (1999) 282–288.
[24] J. Koyama, P.A. Ray-Sequin, R.H. Falk, Prognostic significance of ultrasound myocardial tissue characterization in patients with cardiac amyloidosis, Circulation 106 (2002) 556–561.
[25] J. Koyama, R. Davidoff, R.H. Falk, Longitudinal myocardial velocity gradient derived from pulsed Doppler tissue imaging in AL amyloidosis: a sensitive indicator of systolic and diastolic dysfunction, J. Am. Soc. Echocardiogr. 17 (2004) 36–44.
[26] J. Koyama, R.H. Falk, Prognostic significance of strain Doppler imaging in light-chain amyloidosis, JACC Cardiovasc. Imaging 3 (2010) 333–342.
[27] P. Hammarström, R.L. Wiseman, E.T. Powers, J.W. Kelly, Prevention of transthyretin amyloid disease by changing protein misfolding energetics, Science 299 (2003) 713–716.
[28] A. Yoneyama, J. Koyama, T. Tomita, et al., Relationship of plasma brain-type natriuretic peptide levels to left ventricular longitudinal function in patients with congestive heart failure assessed by strain Doppler imaging, Int. J. Cardiol. 130 (2008) 56–63.
[29] M. Nordlinger, B. Magnani, M. Skinner, R.H. Falk, Is elevated plasma B-natriuretic peptide in amyloidosis simply a function of the presence of heart failure? Am. J. Cardiol. 96 (2005) 982–984.
[30] R.M. Lang, M. Bierig, R.B. Devereux, et al., Recommendations for chamber quantification: a report from the American Society of Echocardiography's Guidelines and Standards Committee and the Chamber Quantification Writing Group, developed in conjunction with the European Association of Echocardiography, a branch of the European Society of Cardiology, J. Am. Soc. Echocardiogr. 18 (2005) 1440–1463.

[31] C. Soullier, P. Obert, G. Doucende, et al., Exercise response in hypertrophic cardiomyopathy: blunted left ventricular deformational and twisting reserve with altered systolic–diastolic coupling, Circ. Cardiovasc. Imaging 5 (2012) 324–332.
[32] A.A. Young, H. Imai, C.N. Chang, L. Axel, Two-dimensional left ventricular deformation during systole using magnetic resonance imaging with spatial modulation of magnetization, Circulation 89 (1994) 740–752.
[33] H. Vogelsberg, H. Mahrholdt, C.C. Deluigi, et al., Cardiovascular magnetic resonance in clinically suspected cardiac amyloidosis: noninvasive imaging compared to endomyocardial biopsy, J. Am. Coll. Cardiol. 51 (2008) 1022–1030.
[34] P.P. Sengupta, A.J. Tajik, K. Chandrasekaran, B.K. Khandheria, Twist mechanics of the left ventricle, JACC Cardiovasc. Imaging 1 (2008) 366–376.
[35] E. Arbustini, L. Verga, M. Concardi, G. Palladini, L. Obici, G. Merlini, Electron and immuno-electron microscopy of abdominal fat identifies and characterizes amyloid fibrils in suspected cardiac amyloidosis, Amyloid 9 (2002) 108–114.
[36] S. Bokhari, A. Castaño, T. Pozniakoff, S. Deslisle, F. Latif, M.S. Maurer, (99m)Tc-pyrophosphate scintigraphy for differentiating light-chain cardiac amyloidosis from the transthyretin-related familial and senile cardiac amyloidoses, Circ. Cardiovasc. Imaging 6 (2013) 195–201.